Translational Oncology 66 (2026) 102690

Contents lists available at ScienceDirect

Translational Oncology

journal homepage: www.elsevier.com/locate/tranon

CMS subtypes correlate with complete response in trial of neoadjuvant Galunisertib plus chemoradiation in rectal cancer

Venkatesh Rajamanickam [a], Noah D. Simons [a], Wesley Rosales [a], Anton Kravchenko [a], Tomoko Yamazaki [a], Brady Bernard [a], Brian Piening [a], Enric Domingo [b], Timothy Maughan [b,c], Charlems Alvarez-Jimenez [d,e], Thomas Desilvio [d], Satish Viswanath [d,f], Mark Whiteford [g], Amanda Hayman [g], David O'Brien [g], Maria X. Kiely [g], Rehan Ahmad [g], Michael J. Gough [a], Marka R. Crittenden [a,h], Kristina H. Young [a,h,*]

[a] Earle A. Chiles Research Institute, Providence Cancer Institute, Portland, OR 97213, USA
[b] Department of Oncology, Medical Sciences Division, University of Oxford, Old Road Campus Research Building, Roosevelt Drive, Oxford, OX3 7DQ, UK
[c] Department of Molecular and Clinical Cancer Medicine, University of Liverpool, Liverpool, UK
[d] Department of Biomedical Engineering, Case Western Reserve University, Cleveland, OH, USA
[e] Faculty of Engineering, Universidad Militar Nueva Granada, Bogotá, Colombia
[f] Louis Stokes Cleveland Veterans Affairs Medical Center, Cleveland, OH, USA
[g] The Oregon Clinic, Colorectal Surgery Division, Portland, OR 97213, USA
[h] The Oregon Clinic, Radiation Oncology Division, Portland, OR 97213, USA

ARTICLE INFO

Keywords:
Rectal cancer
Transforming growth factor beta
Consensus molecular subtypes
Biomarkers

ABSTRACT

Improving responses to neoadjuvant therapy for patients with locally advanced rectal cancer has the potential to improve organ preservation and disease-free survival. Knowing which patients may need therapeutic escalation or de-escalation from standard-of-care treatment remains an area of investigation. We previously reported the primary and secondary endpoints of our single-arm study combining transforming growth factor beta receptor inhibitor, Galunisertib, with neoadjuvant chemoradiation in patients with locally advanced rectal cancer. Here we analyze RNA sequencing data obtained from tissue biopsies at baseline and after 2 weeks of galunisertib. Differences in expression of genes associated with MYC, inflammation, and epithelial-to-mesenchymal transition were observed between complete responders (CR) and <CR, with galunisertib upregulating *MYC* pathway expression in CR. Radiosensitivity and TGFβ response scores demonstrated limited ability to predict for response to galunisertib + chemoradiation. Typically treatment-resistant consensus molecular subtype 4 (CMS4), characterized by TGFβ expression, and metabolic subtype (CMS3) were associated with response to galunisertib + chemoradiation. Differences in correlations between RNA based measures of cell composition and immunohistologic quantification of infiltrates and extracted MRI parameters were observed for CIBERSORT, MCPcounter, and xCell methodologies. Based on these data, we hypothesize that the stromal radioresistant phenotype driven by TGFβ can be overcome by the addition of galunisertib to chemoradiation in rectal cancer.

Research in context:

We previously reported the primary and secondary endpoints of our single-arm Phase II trial of transforming growth factor beta (TGFβ) type I receptor inhibitor, galunisertib, with neoadjuvant chemoradiation in patients with locally advanced rectal cancer. Complete response rate exceeded our predetermined statistical threshold based on historic controls. We now report an exploratory analysis using bulk RNA sequencing of biopsy samples obtained at baseline and after 2 weeks of galunisertib. Differential gene expression analysis, pathway enrichment, and transcription factor activity identified alterations in MYC signaling with galunisertib were associated with complete response consistent with predictors of radiation sensitivity in rectal cancer. Using consensus molecular subtypes (CMS), complete responders were classified as CMS3 and CMS4. The chemo- and radioresistant phenotype, CMS4, driven by TGFβ, was the most frequent baseline CMS phenotype in complete responders. We demonstrate a patient selection rationale for TGFβ inhibition in combination with chemoradiation. In this study, we found patients for whom standard-of-care modalities typically result in poor disease-free survival strongly benefited from the addition of galunisertib.

* Corresponding author at: Earle A Chiles Research Institute, 4805 NE Glisan, Portland, OR 97213, USA.
E-mail address: Kristina.Young@providence.org (K.H. Young).

https://doi.org/10.1016/j.tranon.2026.102690
Received 20 November 2025; Received in revised form 12 January 2026; Accepted 25 January 2026
Available online 6 February 2026

Introduction

Approximately 47,000 cases of rectal cancer are diagnosed in the United States each year. Definitive management for patients with Stage II-III disease typically involves neoadjuvant chemoradiation. Response rates to chemoradiation vary, with complete responses occurring in 8–25 %[1,2]. Pathologic complete response (pCR) rates are associated with fewer local recurrences and greater likelihood of disease-free survival[1]. Increasing the time interval from completion of chemoradiation to surgery was attempted to improve response rates, however in order to prevent delays in care, mFOLFOX6 chemotherapy was administered after chemoradiation, prior to surgery[3]. Based on the slightly improved pCR rates and similar toxicity profile, the sequencing of mFOLFOX6 chemotherapy and chemoradiation (termed total neoadjuvant therapy or TNT) prior to surgery was evaluated in a randomized Phase II trial, demonstrating higher pCR rates with chemoradiation first followed by chemotherapy[4]. The improved response rates prompted an evaluation of whether organ preservation via omission of total mesorectal excision was feasible. At 5 years median follow up, organ preservation was feasible in 54 % of patient who underwent chemoradiation followed by mFOLFOX6[5]. Efforts to better determine which patients are likely to respond or not to chemoradiation would allow for dose escalation or de-escalation strategies to improve patient outcome and minimize toxicity.

Leveraging existing datasets, many groups have proposed putative biomarkers for response to chemoradiation. Colorectal cancer has been subclassified into 4 consensus molecular subtypes (CMS) – CMS1 (MSI Immune), CMS2 (Canonical), CMS3 (Metabolic), and CMS4 (Mesenchymal). The CMS1 subtype comprises approximately 3 % of rectal cancers and is characterized by hypermutation, BRAF mutations, immune infiltration and activation[6]. The CMS2 phenotype makes up approximately half of rectal cancers and is associated high levels of somatic copy number alterations (SCNA) with WNT and MYC activation [6]. Approximately 15 % of rectal cancers classify as the CMS3 subtype, characterized by metabolic deregulation, KRAS mutations, low levels of SCNA, and CpG Island Methylator Phenotype Low[6]. While about 30 % of rectal cancers are classified as CMS4, characterized by high levels of SCNA, stromal immune infiltration, transforming growth factor beta (TGFβ) activation, and angiogenesis[6]. Across all colorectal cancer, CMS4 phenotype has the worst overall survival and relapse-free survival, while CMS1 has the worst survival after relapse[6]. When evaluating response to chemoradiation by CMS subtype, CMS1 has the highest likelihood for pCR*(2* [7],. This is consistent with improved survival outcomes and chemoradiation response observed for colorectal cancer patients with high levels of immune infiltrates[8–10], a feature of the CMS1 phenotype. By contrast, the least likely CMS group to achieve pCR with 5-fluorouracil based neoadjuvant chemoradiation was CMS4 [11,7]. Consistent with this, F-TBRS, a fibroblast TGFβ signature, strongly associated with lack of pCR[11]. TGFβ is a multipotent cytokine with roles in angiogenesis, EMT, invasion and metastasis[12], and is a dominant immunosuppressive cytokine in the tumor microenvironment [13–16] associated with immune exclusion and resistance to immune checkpoint blockade[17]. We developed a clinical protocol that translated our preclinical work demonstrating TGFβ type I receptor inhibition improved tumor immune infiltrate prior to radiation resulting in improved radiation response[14,18].

We previously published the results of our single-arm Phase II clinical trial of transforming growth factor beta (TGFβ) type I receptor inhibitor, Galunisertib, in combination with chemoradiation in locally advanced rectal adenocarcinoma (NCT02688712)[19]. Enrolled patients received galunisertib for 2 weeks prior to starting 5-FU based chemoradiation (**Supplementary Figure 1**). Since galunisertib is dosed 2 weeks on and 2 weeks off, patients received a total of 2 cycles of galunisertib, with the second cycle concurrent with chemoradiation (**Supplementary Figure 1**). The primary endpoint was complete response (CR) defined as pathologic complete response or clinical complete response at 1 year after completion of therapy for patients who underwent non-operative management. Thirty-two percent of patients achieved a CR to neoadjuvant treatment, exceeding our predetermined statistical threshold[19]. Of those who pursued non-operative management, and therefore had total neoadjuvant therapy, 70 % had a CR[19]. Planned secondary endpoints included peripheral blood immune monitoring and immunohistochemical analysis of immune cell infiltrate from biopsy samples obtained at baseline and day 15 (after 2 weeks of galunisertib alone), and surgical specimens (obtained 6–10 weeks following galunisertib + chemoradiation). As reported previously, we observed a reduction in activated CD8+ effector-memory T cells in the peripheral blood of complete responders (CR) compared to patients who did not achieve a complete response (<CR)[19]. Additionally, loss of peripheral blood CXCR3+ CD8+ T cells correlated with response to therapy and increased CXCR3+CD8+ T cells infiltrating the tumor[19], consistent with preclinical work demonstrating TGFβ regulation of CXCR3 expression on CD8 T cells influencing tumor-homing[14]. While there was no statistical differences in tumor immune infiltrate quantified by multiplex immunohistology, trends towards increased CD4+ T cells and reduced regulatory T cells and macrophages were observed in patients with CR[19]. Patients on study also underwent multiparametric MRI at baseline (day 0) and following the first 2 weeks of TGFβ inhibition (day 15). Exploratory analysis of MRI parameters demonstrated correlation with treatment response and CD8+ and macrophage tumor infiltration[20].

Here we report a new exploratory analysis of bulk RNAseq data obtained from patients enrolled on study NCT02688712 at baseline and after two weeks of TGFβ inhibition. We describe differentially expressed genes and pathways enriched in patients with complete response. We evaluate RNA based measures of cellular composition and correlate these with multiplex IHC based cell counts and MRI based imaging parameters. We evaluate whether prior metrics of chemoradiation response including RSS and F-TBRS are valid in our cohort. Finally, we report that typically chemoradiation resistant CMS4 phenotypes, characterized by high TGFβ signaling, are associated with complete response in our cohort suggesting addition of TGFβ inhibition in these patients could improve rates of organ preservation and potentially disease-free survival.

Materials and methods

Study design

Patients with locally advanced rectal cancer for whom neoadjuvant chemoradiation was the standard of care, were offered participation in single-arm, Phase 2 clinical trial NCT02688712 evaluating the addition of Galunisertib to chemoradiation (**Supplementary Figure 1**). Primary study design and endpoints were previously published[19]. Herein, we report exploratory endpoints utilizing bulk RNAseq of biopsy samples. Forceps biopsies were obtained at baseline (Day 0) and after 2 weeks of Galunisertib (Day 15) (±3 days), and stored in RNAlater. Of the 38 enrolled patients, 37 underwent study treatment. Therefore 74 samples were obtained for RNAseq analysis. Library preparation and RNA sequencing were successful in 73 of 74 samples. Quality control metrics were acceptable for the 73 samples (n=36 at day 0, n=37 at day 15).

Library prep

Total RNA were purified from forceps biopsy specimens stored in RNALater using DNA/RNA AllPrep reagents (Qiagen) according to the manufacturer's instructions. Library preparation using the Illumina TruSeq RNA Exome kit converts total RNA into a library of known strand origin, and then capture the coding regions of the transcriptome using the following workflow.

The RNA is fragmented using divalent cations under elevated temperature. cDNA is generated from the cleaved RNA fragments using

random priming during first and second strand synthesis. Then, sequencing adapters are ligated to the resulting double-stranded cDNA fragments. The coding regions of the transcriptome are captured from this library using sequence-specific probes to create the final library. Captured library pools were normalized and loaded onto a Illumina Novaseq 6000 for sequencing.

RNA preprocessing

RNA sequencing reads were aligned to GRCh38 human reference genome, and transcript-level expression was quantified using Salmon v0.12.0[21]. A total of 175,775 transcripts corresponding to over 20, 598 genes were initially detected. Transcript-to-gene level summarization was performed using the tximport package in R. Transcripts per million (TPM) values were used as input for immune cell deconvolution analyses with xCell[22], CIBERSORT[23], and MCPcounter[24].

QC and differential expression analysis

73 samples passed sequencing QC and 1 sample failed QC (TGF01 Day 0). Normalization and differential gene expression analysis were conducted using limma[25] and edgeR[26]. Genes with a maximum counts per million (CPM) value below 20 across all samples were excluded from the analysis, resulting in 12,932 genes for downstream analyses.

Celltype deconvolution

Cell type deconvolution was performed using xCell[22], MCPcounter [24], and CIBERSORT[23], with TPM gene expression levels as input. xCELL was used to perform cell type enrichment analysis from gene expression data for 64 immune and stroma cell types, whereas CIBERSORT provides absolute and relative abundance of different immune cell types depending on the specified gene set. In the present analysis, the LM22 signature provided by CIBERSORT was applied. We used MCPcounter to estimate the abundance of immune cell population. MCPcounter quantifies abundance of tissue-infiltrating eight immune and two stromal cell populations based on transcriptome profile.

Principal component analysis and heatmaps

Principal component analyses and heatmaps were generated using the ClustVis tool (https://biit.cs.ut.ee/clustvis/).

Transcription factor activity enrichment

Transcription factor activity was calculated using the decoupleR (v2.10.0)[27] R package. CollecTRI[28] regulons and DGE t-values were input into the run_mlm function to get transcription factor activity enrichment scores. The run_mlm function fits a multivariate linear model for each sample and calculates how well the given transcription factor's regulon weights can predict the given t-values. The function then generates an additional t-value that is interpreted as the enrichment score.

Molecular subtyping

Predicted Consensus Molecular Subtype (CMS) classifications were calculated based on gene expression data via the CMScaller function with default settings implemented in the CMScaller R package[29].

MRI parameters

Patients on study underwent multiparametric MRI at baseline (day 0) and following the first 2 weeks of TGFβ inhibition (day 15).MRI parameters were obtained as described in [20]. Day 0 parameters were available on 36 patients. Day 15 parameters were available on 19 patients.

Statistics

Data was analyzed using GraphPad Prism. Comparisons between groups or timepoint were performed using *t*-tests or ANOVA. Fisher exact test was used to compare treatment outcomes with experimental parameters (e.g. radiosensitivity signature). For correlation matrices, Pearson correlations were calculated with r and p-values reported. False discovery rate corrections to correlation p-values were performed using the Benjamini and Hochberg method with a false discovery rate of 30 %.

Role of the funding source

The clinical trial was partially funded through the ExIST mechanism from Eli Lilly and Company, who owned Galunisertib, and provided the study drug. The remainder of the study was funded by The Providence Foundation. The sponsors had no role in study design, collection, analysis, or interpretation of the data; in the writing of the report; nor in the decision to submit the paper for publication.

Results

Patients with locally advanced rectal cancer for whom neoadjuvant chemoradiation was the standard of care, were offered participation in single-arm, Phase 2 clinical trial NCT02688712 evaluating the addition of Galunisertib to chemoradiation (**Supplementary Figure 1**). We have previously published the primary and secondary endpoints including favorable safety profile, clinical efficacy (a complete response rate of 32 %), peripheral blood immune monitoring data, and multiplex immunohistochemistry data. Herein, we report exploratory endpoints utilizing bulk RNAseq of biopsy samples. Forceps biopsies were obtained at baseline (Day 0) and after 2 weeks of Galunisertib (Day 15) (±3 days), and stored in RNAlater. Of the 38 enrolled patients, 37 underwent study treatment. Therefore 74 samples were obtained for RNAseq analysis. Library preparation and RNA sequencing were successful in 73 of 74 samples. Quality control metrics were acceptable for the 73 samples.

Gene expression and signaling pathway changes

Differentially expressed genes were evaluated at day 0 and day 15 comparing complete responders (CR) to those who had less than a complete response (<CR). At day 0, CR had alteration of genes associated with inhibition of MYC signaling, mTOR signaling, inflammation, epithelial-to-mesenchymal transition (EMT), and metabolism (**Supplementary Figure 2A-B,** Table 1A-B). Conversely, at day 15, after 2 weeks of TGFβ inhibition, complete responders demonstrated gene alteration associated with upregulation of MYC signaling, but consistently demonstrated downregulation of the NFKB pathway, inflammation, EMT, and hypoxia (**Supplementary Figure 2C-D,** Table 2A-B). While CR at day 0 downregulated pathways associated with glycolysis, at day 15 they downregulated pathways associated with fatty acid oxidation, suggesting a change in metabolic processes (**Supplementary Figures 2A-D**). Several upregulated genes noted in Table 2A-B are associated with antigen presentation (TAP2 and HLA-DRs) and vascular activation (CHST4) suggesting immune potential. Next, we queried the impact of TGFβ inhibition by evaluating the change in gene expression within each patient from day 0 to day 15, then comparing CR to <CR (Fig. 1A-**B,** Table 3A-B). In this analysis, CR demonstrated significant upregulation of pathways associated with NFKB signaling, interferon signaling, and inflammatory responses, while down-regulating EMT, consistent with the expected impact of TGFβ inhibition. To further evaluate the impact of TGFβ inhibition on gene expression, we compared day 15 versus day 0, without respect to responder status (**Supplementary Figure 2E-F**, Table 4A-B). Interestingly, there is upregulation of

Table 1A
Upregulated in CR at baseline.

Up in CR	Log_2FC	$-log_{10}$ P-value
IGHV3–15	3.680692353	1.923821909
IGHV3–21	3.546180414	2.867027321
INSL5	3.251673608	2.068184416
HLA-A	3.232566948	1.879004416
CA1	3.070769828	1.795067074
CA4	2.88729395	2.568515615
ZG16	2.855055644	1.717400882
CLCA4	2.830305957	1.946920826
CLDN8	2.823247277	1.313107037
IGHV3–74	2.744637748	1.697372333
SI	2.728844996	2.184448549
SLC30A10	2.71941202	2.082169128
TMIGD1	2.644234798	1.34728986
GCG	2.62038555	1.846298311
MS4A12	2.602604213	1.312493084
PYY	2.5722606	1.733290348
SLC6A19	2.563142691	1.32129759
GUCA2B	2.535815802	1.449984969
ALDH1A2	2.524363254	3.125309493
CD177	2.474681761	1.6405865
HOXD13	2.426202919	1.997706693
CA7	2.411557468	1.743422064
SST	2.35600295	2.118514343
IGHV4–4	2.321797299	2.525020602
ANO5	2.283091369	1.854543717
SULT1E1	2.261808339	1.731284905
GUCA2A	2.253961622	1.743168982
IGHV1–3	2.193863682	1.468235858
SLC4A4	2.180074019	1.5107296
SCNN1B	2.177771286	1.425997953
SLC26A3	2.147260504	1.570060433
TMEM132C	2.139892948	1.592152196
FDCSP	1.995795753	1.592361814
TCL1A	1.976609944	1.721756446
CA2	1.968600478	1.529122431
ABCG2	1.962632593	1.643092559
TRIM31	1.938395474	1.751144908
SERPINB7	1.893926001	1.527271817
HOXA13	1.8931401	1.766345075
HSPA1B	1.849653556	1.977386237
HOXD10	1.838872257	1.944728267
JCHAIN	1.796666138	1.743083284
VSIG2	1.760782161	1.335167616
HOXD11	1.757325108	1.783699448
C11orf86	1.741942646	1.741815179
SELENOP	1.73206319	2.180632845
IGKV1–17	1.723404278	1.380579683
VNN1	1.721675532	2.65457353
BTNL8	1.711941348	2.262264749
GPAT2	1.705490037	2.34947315
TRANK1	1.678914374	1.90261374
SCGB2A1	1.661073559	1.337553253
LYPD8	1.655633976	1.806157655
DHRS9	1.644272619	1.948745884
IGLV2–8	1.634327143	1.724881852
BTNL3	1.624308856	2.136170382
ALPI	1.587474274	1.390626689
EVX1	1.560423926	1.698222207
IGHA1	1.559518936	1.563987314
CEACAM7	1.517988876	1.395367661
THRB	1.505165025	1.634315822
CIDEC	1.495578019	1.522164296
AKR1B10	1.467234962	1.507404339
USP2	1.45527924	2.299032412
TRPM6	1.45196534	1.329174241
IGHV4–61	1.45146834	1.378104476
REEP1	1.442589408	1.531899874
TM4SF20	1.413588874	1.33806798
CDKN2B	1.378596347	1.558924706
MMP28	1.377924417	1.658338495
HOXB13	1.375321491	1.351670644
ABCB1	1.338692307	1.70090455
LGALS2	1.310580087	1.426658186
HPGD	1.307698526	1.536270104

Table 1A (*continued*)

Up in CR	Log_2FC	$-log_{10}$ P-value
HOXD9	1.289531704	1.515299456
PKIB	1.264369027	1.847570686
PDK4	1.259645061	2.135016377
SLC51B	1.243955894	1.607775401
PCDH19	1.211162213	1.345932797
TBX10	1.205402016	1.426788399
CDHR2	1.198565946	2.352661244
XDH	1.193417324	1.868281145
CASP5	1.178450545	1.876675743
TSPAN1	1.166462218	1.808359296
DPP4	1.16312411	1.647237073
LTK	1.140809684	1.354020698
BAMBI	1.128466304	1.693302814
GPT	1.087127564	1.4052001
GDA	1.078946689	2.442806662
SLCO2A1	1.073799104	1.679411001
ISX	1.072239888	1.716093895
SYTL5	1.06634314	1.334768311
ZNF813	1.063334045	2.182606862
MALL	1.06083464	1.442998582
KCND3	1.057960047	1.459694231
GCNT3	1.043153633	1.391234283
SAMD9	1.039231754	1.701825258
SMPDL3A	1.010856996	1.37156421
MT-ND3	1.009092638	2.587602627
SECTM1	1.001850942	1.316898048

Table 1B
Downregulated in CR at baseline.

Down in CR	Log_2FC	$-log_{10}$ P-value
INPP5D	-1.017	1.777443285
BEX3	-1.065	1.521209879
PGBD5	-1.1242	1.487180655
XKRX	-1.1435	1.483606572
ALOX15B	-1.2077	1.320164458
MAPK15	-1.2211	1.339143189
IGFBP2	-1.2888	1.326990748
EPHX3	-1.3467	1.524753597
RPL17-C18orf32	-1.4518	1.411198172
MBOAT7	-1.4735	1.744230825
FGD1	-1.5971	1.739857651
CCNP	-1.6569	1.355376269
IL36G	-1.7289	1.73226633
PADI3	-2.4215	1.782136043
ARC	-2.476	2.983092374
ZBTB22	-2.8798	1.343603704
KLK8	-3.4702	1.997910778

several hallmark pathways (**Supplementary Figure 2F**), but no pathways are downregulated. Consistent with Fig. 1B, there is upregulation of TNFa signaling, inflammation, complement, IL6/STAT3, apoptosis, IL2/STAT5, and heme metabolism, suggesting shared mechanisms that are more exaggerated in CR than <CR. However, unique pathways in Fig. 1B that are not observed in **Supplementary Figure 2F** include downregulation of E2F, EMT, and myogenesis, the latter of which were on average upregulated at Day 15. Additionally, hypoxia pathways, which should skew towards radioresistance, were upregulated in CR vs <CR (Fig. 1B), but no differences were observed when considering all patients (**Supplementary Figure 2F**). Increased metabolism was seen at day 15 including oxidative phosphorylation and fatty acid metabolism (**Supplementary Figure 2F**). Finally, at day 15 MYC and KRAS pathways were upregulated (**Supplementary Figure 2F**). Together these data suggest that Galunisertib impacted cellular metabolism, inflammation, and signaling pathways, while complete responders downregulated EMT and upregulated interferon pathways.

Based on the change in MYC pathway activity in responders between day 0 and day 15 (**Supplementary Figure 2B,D**), we performed a transcription factor activity analysis. There was increased MYC activity

Table 2A
Upregulated in CR at Day 15.

Up in CR	Log_2FC	$-log_{10}$ P-value
TAP2	4.144366884	2.283873907
HLA-DRB5	3.523610184	2.536548206
HLA-DRA	3.463796131	1.650859546
PRRC2A	3.363056345	1.399736293
UBD	3.269176227	1.676018996
PPP1R11	2.889007791	1.795481223
TRIM15	2.622975791	1.448284716
SOX2	2.610424167	2.765436815
CHST4	2.563150527	1.695133654
TRIM71	2.491390574	2.206933127
SIM2	2.475933221	3.631962785
WDR46	2.411578253	2.142471886
FOXC1	2.395791838	1.681602042
TMEM178B	2.32666174	2.51722239
IGF2	2.258771231	1.729015294
GAL	1.75445946	1.46619442
SCN2A	1.748556178	1.611053938
LGR6	1.706699103	2.629219717
NEB	1.541214328	1.497215679
ARHGEF35	1.46627397	1.676897056
LPAR3	1.455090345	2.166081068
PRODH	1.435623078	1.821872251
VARS1	1.391007109	1.711958694
SNCAIP	1.388270785	2.08823143
IGF2BP3	1.362104404	1.684740104
PNPLA3	1.360288833	1.556914967
RNF183	1.327016351	1.983069299
HHLA1	1.311536362	1.524124585
PWP2	1.257511133	1.393977436
ABHD12B	1.18950343	1.501834903
NKD2	1.1806073	1.533232724
PUF60	1.172118755	1.720314078
SULT1C4	1.15828535	1.344931919
ONECUT3	1.140938602	1.535168692
GRIN2B	1.0706943	1.61508428
NHS	1.062552294	3.247694236

Table 2B
Downregulated in CR at Day 15.

Down in CR	Log_2FC	$-log_{10}$ P-value
OASL	-1.0056	1.526569874
DDX60	-1.0092	2.095597357
PDK4	-1.0177	1.481276277
SLC16A14	-1.0334	1.676872844
F13A1	-1.0438	1.571735547
KCND3	-1.0622	1.352687277
ST6GALNAC3	-1.063	1.52872084
KRT20	-1.0808	1.384424489
HDGFL3	-1.0894	1.584587151
CPM	-1.0915	1.304916638
MMRN1	-1.0925	1.395483817
ACHE	-1.1132	1.426604608
HSD17B2	-1.1587	1.464385432
PLA2G10	-1.1617	1.518645008
GBP3	-1.2225	1.681080041
CMPK2	-1.2235	2.077181015
SAMD9	-1.2348	2.282795066
SECTM1	-1.2457	1.693464017
PPARGC1A	-1.2781	1.864589414
SIGLEC14	-1.3027	1.580648343
IGLV2–11	-1.3239	1.325785818
IGLV3–1	-1.3287	1.704144066
TMEM220	-1.3489	1.549549232
C7	-1.3637	1.658938925
WSCD1	-1.3991	1.712294989
IGHV3–53	-1.4004	1.433034993
B3GALT1	-1.4054	1.315995896
IGKV1–9	-1.4292	1.30830983
BTNL3	-1.4597	1.814222285
MUC12	-1.5373	1.83403502
TSEN34	-1.5967	1.912991022
CAPN14	-1.6221	1.643364004
FIBCD1	-1.7206	1.443004056
IGLV6–57	-1.7266	1.699339987
RSAD2	-1.7566	1.965492813
B3GNT6	-1.7679	1.364633243
BTNL8	-1.7726	1.981791298
ST6GAL2	-1.7766	1.722990487
LDHD	-1.7918	1.800794595
ALPI	-1.9632	1.791982018
TRANK1	-1.9661	1.999724269
IGHV3–33	-1.974	1.646570449
SCNN1G	-2.0321	1.361802327
IGHV1–2	-2.0538	1.458081483
IGHV1–69	-2.0583	1.509874495
CA2	-2.2431	1.900608423
CA4	-2.2577	1.705398815
IGHV1–69D	-2.2594	1.344472955
SCNN1B	-2.2666	1.584172861
GCG	-2.4304	1.543119964
INSL5	-2.4761	1.428191523
CA1	-2.6071	1.306528246
ANO5	-2.687	1.583789534
ZG16	-2.6953	1.657605735
IGHV3–21	-2.7453	2.051381193
CLCA4	-2.8936	1.914736244
IGHV3–43	-3.614	3.807745659

in non-CR at day 0 (**Supplementary Figure 3A**). This was associated with differential gene expression of MYC associated target genes (**Supplementary Figure 3B**). Consistent with our pathway analysis, at day 15, we saw an upregulation of MYC activity in complete responders (**Supplementary Figure 3C**). Alteration of MYC pathway target genes demonstrated reciprocal expression patterns compared to baseline measures. Previously published analyses have demonstrated increased MYC pathway activity correlates with complete response to neoadjuvant chemoradiation in rectal cancer*(2)*. Our data would suggest that two weeks of TGFβ inhibition were sufficient to flip MYC activity promoting improved responsiveness to chemoradiation.

Radiosensitivity and TGFβ responsesignatures

Previous studies demonstrated response to neoadjuvant chemoradiation in rectal cancer was predicted by a 33-gene signature termed the radiosensitivity score (RSS), where higher values correspond to better response to chemoradiation*(2)*. Pathway analysis of the RSS included upregulation of inflammatory pathways and MYC targets, and downregulation of EMT*(2)*. We evaluated whether RSS predicted response in our cohort of patients and found that patients with CR had a higher average RSS, but this did not reach statistical significance (Fig. 2A, Day 0: 0.5037 [CR] vs 0.4254 [<CR], NS; Day 15: 0.5687 [CR] vs 0.5037 [<CR], NS). Using a midpoint cutoff of 0.5 (RSS range is 0–1), the RSS failed to predict complete response at baseline (Fig. 2**Bi**, Fisher exact test, p=0.1410), at day 15 (Fig. 2**Bii**, Fisher exact test, p=0.4821), or combined for all time points (Fig. 2**Biii**, Fisher exact test, p=0.0746). Given that pathways associated with EMT are strong drivers of a low RSS, we predicted that inhibition of TGFβ, a major driver of EMT pathways, may negate the predictive validity of this biomarker.

Based on the role of TGFβ in regulating the tumor stroma, we subsequently evaluated for differences in the fibroblast TGFβ response signature (F-TBRS) which was previously shown to predict response to neoadjuvant chemoradiation*(2)*. No significant differences were seen in F-TBRS scores between CR and <CR (Fig. 2C, Day 0: 0.03619 [CR] vs 0.0006110 [<CR], NS; Day 15: 0.1130 [CR] vs -0.07078 [<CR], NS). Using the published cutoffs for low, medium, or high expression[30], there was no association with F-TBRS and CR at baseline (Fig. 2**Di**, Fisher exact test, p=0.6399), day 15 (Fig. 2**Dii**, Fisher exact test, p=0.2236), or at all time points combined (Fig. 2**Diii**, Fisher exact test, p=0.1255). Fourteen patients F-TBRS score changed from baseline to day 15 (3 CR and 11 <CR), six patients score increased to a higher category (1 CR and 5 <CR), eight decreased to a lower category (2 CR and 6 < CR). Direction or magnitude of change in F-TBRS did not correlate with response (Fig. 2C and data not shown). Based on these

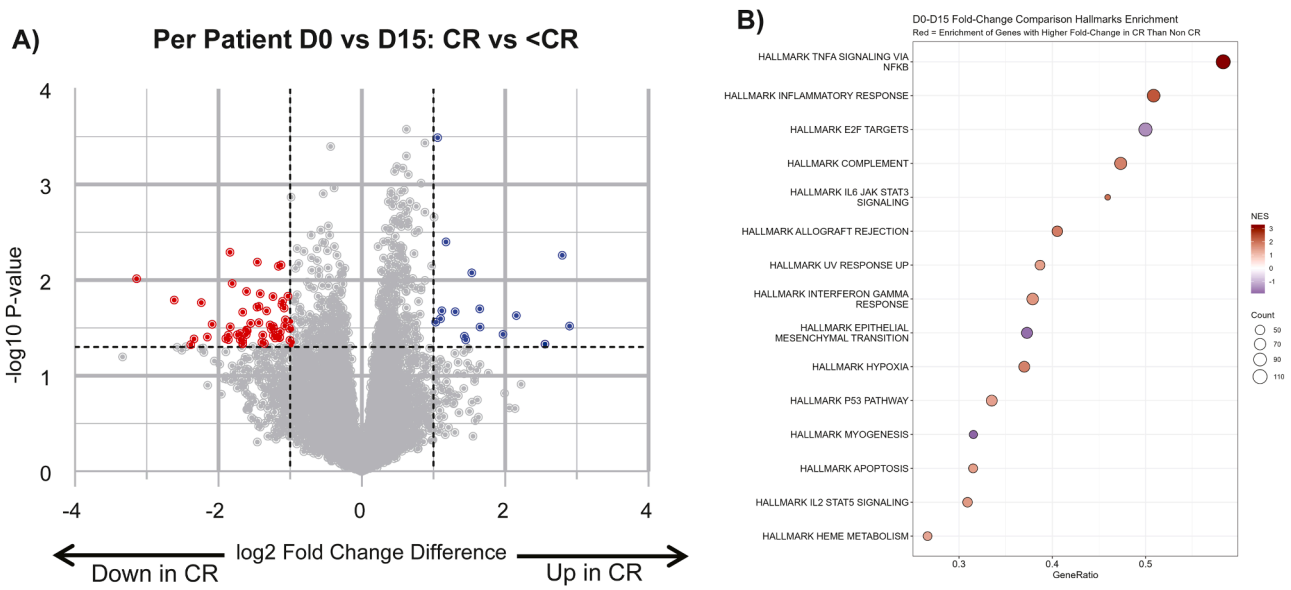

Fig. 1. Complete response associated with upregulation of inflammatory pathways and downregulation of epithelial-to-mesenchymal transition pathways. A) Difference in gene expression between Day 15 (D15) and day 0 (D0) within each patient, comparing CR vs <CR. Upregulated genes in CR shown on the right (blue), downregulated genes in CR shown on the left (red). B) Hallmark pathway analysis of pathways altered between D15 and D0 per patient corresponding to (A). Upregulated pathways are shown in red, size of circle reflects size of effect.

Table 3A
Increased between baseline and Day 15 in CR.

Up in CR	Delta Log_2FC	$-log_{10}$ P-value
HBA1	2.899489425	1.520020658
PAH	2.796091411	2.263179341
EDNRA	2.558196192	1.332398718
PKLR	2.159122935	1.630182263
SKIV2L	1.972034676	1.433740132
TBC1D3L	1.65127389	1.512361546
KIF26B	1.648568486	1.701356602
DLC1	1.534502859	2.077646807
ITGA11	1.451309525	1.377274911
ELN	1.435279051	1.415671224
ABHD16A	1.304479208	1.673081376
CCDC183	1.175822315	2.401851969
CRB2	1.116806821	1.680786099
HSF4	1.100504889	1.598703515
LZTR1	1.060088589	3.492242567
SLC19A3	1.034189908	1.561238409
AMT	1.009059839	2.657285546

data, the addition of a TGFβ inhibitor invalidates the inverse correlation between F-TBRS and response to neoadjuvant chemoradiation. In fact, a higher percentage of patients with complete response had a medium or high F-TBRS (91 %) compared to <CR (75 %). We next evaluated TGFβ response signatures in T cells (T-TBRS), macrophages (M-TBRS), and endothelial cells (E-TBRS). We observed no significant differences between CR and <CR in any of these signatures at baseline or day 15 (**Supplementary Figure 3A-F**). However, there was a significant association between high/medium endothelial TGFβ response signature (E-TBRS) and complete response when all time points were combined (**Supplementary Figure 3Fiii**, Fisher exact test p=0.0253), and a trend towards significance with all timepoints combined for the macrophage signature (M-TBRS, **Supplemental Figure 3Diii**, Fisher exact test p=0.0512). These data suggest complete response to neoadjuvant chemoradiation plus galunisertib is more frequent in patients with high/-medium stromal TGFβ expression.

Analysis of immunecellinfiltration

We subsequently performed RNA based cell quantification using CIBERSORT, MCPcounter, and xCELL. In our prior publication, we quantified infiltrating CD4+ T cells, CD8+ T cells, regulatory T cells, and Macrophages using multiplex immunohistology. We found no statistical association between cell counts and complete response, though there were trends towards reduced regulatory T cells and macrophages in responders[19]. We evaluated whether RNA-based cell quantifications were consistent with immune cell counts from multiplex immunohistology. The immune cell density data from forceps biopsy specimens was obtained concurrently with tissue stored in RNAlater for this analysis[19]. Very few correlations were observed between mIHC and RNA-based methods (Fig. 3). Each algorithm had a few successes: CIBERSORT was able to predict CD4+ T cells at baseline (Fig. 3**Ai**, R^2=0.15, p=0.0251 [CD4 resting memory], R^2=0.16, p=0.0192 [CD4 Sum] and CD8+ T cells at day 15 (Fig. 3**Aii,** R^2=0.27, p=0.0014 [CD8]; MCPcounter has no significant correlations; and xCell significantly correlated with of CD4+ memory T cells (Fig. 3**Bi,** R^2=0.27, p=0.015), CD8+ central memory T cells (Tcm) (Fig. 3**Bii,** R^2=0.16, p=0.019), and M1 macrophages (Fig. 3**Biii,** R^2=0.17, p=0.013) all at day 15. We then compared whether the different deconvolution methods correlated with one another. Generally, there was stronger agreement between xCell and MCPcounter, particularly in monocyte, macrophage, and dendritic cell estimations (**Supplementary Tables 1–3**). CIBERSORT estimations of CD8+ T cells correlated with xCell CD8+ T cells, CD8+ effector memory (CD8+ Tem) and naïve CD8+ T cells, while it correlated with both CD8 T Cells and T cell estimates by MCPcounter (**Supplementary Table 1A-B**). CIBERSORT measures of CD4 memory resting cells correlated with xCell CD4+ memory cells at day 0 (**Supplementary Table 2A**), while at day 15 the CD4 memory activated estimates correlated with several xCell based measures of CD4 T cells and MCPcounter estimates (**Supplementary Table 2B**). CIBERSORT and xCell measures of M2 macrophages at day 0 and day 15 correlated, while only MCPcounter measures at day 15 correlated with CIBERSORT (**Supplementary Table 3A-B**). CIBERSORT and xCell measures of regulatory T cells did not correlate at either time point(**Supplementary Table 4A-B**).

We have previously published correlations between MRI features

Table 3B
Decreased between baseline and Day 15 in CR.

Down in CR	Delta Log_2FC	$-log_{10}$ P-value
IL6R	-1.0033963	1.374448304
SLC15A1	-1.004462393	1.498272298
MAFF	-1.030649073	1.834206945
SERPI01	-1.062235303	1.587441132
ABCA13	-1.072346356	1.526276199
ADGRF1	-1.076970342	1.314536926
GPAT3	-1.082611479	1.713134266
NFIL3	-1.102969366	1.782570825
AQP3	-1.115136584	1.748911263
SEMA7A	-1.127545628	2.161786142
NFKBIA	-1.13343885	1.464506434
SIK1	-1.144341565	1.408176303
NKX3.1	-1.145615135	1.400949205
DUSP5	-1.160964937	2.149547148
EVI2A	-1.169226687	1.426469919
PFKFB3	-1.207033398	1.399619356
CXCR4	-1.226966808	1.49996304
CD14	-1.232715968	1.516710143
C16orf54	-1.233055039	1.424073777
HMOX1	-1.238822223	1.831264599
TRGC1	-1.26204302	1.493265512
CD55	-1.276668134	1.536063138
CYTIP	-1.326774792	1.682515648
TDRD9	-1.359133418	1.342729424
ALOX5AP	-1.380500025	1.427340454
NR4A3	-1.39445686	1.356308819
PLAUR	-1.413739809	1.861903385
PRKCB	-1.431620612	1.558179619
IL1R2	-1.431972736	1.728462811
ADM	-1.454296319	2.190007673
ANGPTL4	-1.459668631	1.721062431
CAMK1G	-1.517473105	1.309763295
ADORA2A	-1.550965235	1.55282001
PHACTR1	-1.596988723	1.475877218
SRGN	-1.608051963	1.482616357
SH2D1B	-1.608057476	1.883378777
A4GALT	-1.611764753	1.435575659
CD69	-1.657964009	1.668354485
CAPN14	-1.658263089	1.376624113
RIPOR2	-1.658361595	1.338805988
MGAM	-1.658811522	1.346341934
PDE4B	-1.694292487	1.444115511
VNN2	-1.696507712	1.382728465
IL23A	-1.735337069	1.430431785
DSG3	-1.807199477	1.966780174
VNN1	-1.835339646	1.514879234
HSPA6	-1.836938348	2.295094467
PLEK	-1.85936928	1.380939302
BCL2A1	-1.861950018	1.429719878
IL1RN	-1.894234307	1.390748985
G0S2	-2.084587046	1.541682342
SPRR2D	-2.152676206	1.407169713
ALDH1A2	-2.239164959	1.766966584
HCAR2	-2.339609091	1.388537566
PROK2	-2.385055951	1.327064405
SPRR2A	-2.451789563	1.304711777
SLC30A10	-2.616116813	1.795824858
CA4	-3.141971903	2.019208892

Table 4A
Upregulated at Day 15.

Up at D15	Log2 FC	-log10 P-value
DDX39B	3.355606175	2.073663277
KDM5D	2.764185082	1.794262881
DDX3Y	2.736466451	1.700617011
BNIPL	2.38718522	4.76497285
UTY	2.361319866	2.401674795
ZFY	2.331171866	1.776432088
PADI3	2.172032377	3.145948002
USP9Y	1.950962432	2.037802719
MALRD1	1.916524986	2.452931074
SULT1E1	1.773021363	1.779757415
EIF1AY	1.762046763	2.744680654
HSPA1B	1.595638414	2.514235003
CA9	1.561014215	1.706601669
PLA2G3	1.556103304	1.615703922
SLC28A3	1.53316434	3.938398177
ELF5	1.490140418	1.756613764
TFAP2A	1.484590258	2.623026298
PCDHA4	1.418298491	7.617441477
POTEI	1.375397311	2.187654247
POU6F2	1.366829908	4.564508725
RETNLB	1.327365235	1.65951483
CTNNA2	1.312344691	1.710447417
ZNF750	1.304751474	1.643340364
GOLGA6L9	1.30352553	3.617463026
WDR72	1.296110054	2.186957284
SHC2	1.295838663	3.722186305
LRRN1	1.289678148	1.861798587
GABRP	1.254725208	3.182336943
ALDH3B2	1.23677603	2.101916162
NPC1L1	1.228826249	1.684846777
CLDN18	1.203632693	1.641664341
KCNJ3	1.196401186	2.156304926
CBLIF	1.188012962	1.670663697
ADH7	1.166956765	3.474719708
RANBP17	1.154158404	4.502486624
ZNF488	1.145677816	3.003125147
DUOX1	1.144589405	3.624055371
TRIM72	1.133466889	4.058597501
TMEM40	1.127998822	2.633151461
AMER3	1.125811361	3.254740256
CADPS	1.124112883	3.332715532
TMEM45A	1.115667828	5.120157135
PCDHB9	1.114915205	3.91836073
SHISA9	1.099087125	4.073990696
GSDMC	1.092283759	2.109129673
PCDHGA8	1.091212994	3.688952707
CAPN12	1.085736996	2.771023517
CALML3	1.084980787	1.562679108
PLEKHS1	1.083633912	3.723503606
PRDM16	1.08209691	2.571345881
SAA2	1.078169641	2.638678028
CECR2	1.076009071	2.270504772
CATSPERB	1.071845341	4.561346785
EPPIN	1.061395059	3.229617163
CLEC18A	1.056048381	3.548041703
FAM241A	1.036960098	4.495380328
CYP4F8	1.036760252	3.557582731
KLK7	1.032715821	1.82717693
NEB	1.030691203	1.56472252
HHLA1	1.021470728	1.945538976
PNPLA3	1.019932314	1.8732787
PLIN5	1.011497396	3.208153444
ANKRD18A	1.005115934	2.640186704

and immune cell counts by immunohistology at day 15[20]. We found that texture-based features positively correlated with CD8+ T cell counts, while they inversely correlated with macrophage counts[20]. We next assessed whether RNA-based cell counts correlated with MRI features at day 0 or day 15. CIBERSORT measures of CD4+ T cells and myeloid cells (monocytes, M0 macrophages, and dendritic cells) correlated with MRI based measures of the tumor microenvironment (**Supplementary Figure 5A**). MCPcounter based measures of T cells, cytotoxic lymphocytes, and NK cells correlated with MRI based measures at day 15, which is somewhat consistent with correlations to mIHC based cell counts (**Supplementary Figure 5B** and *(22)*). Finally, xCell based measures of CD4+ T cells and monocytes at baseline correlated with MRI based measures, while CD8+ T central memory cells correlated with MRI measures at day 15 (**Supplementary Figure 5C**). After relaxed false discovery rate corrections based on sample size and the exploratory nature of this analysis, we found no significant correlations using MCPCounter or CIBERSORT, but with xCell there remained significant correlations between Day 0 Axial Diffusion-AV and CD4+ Tcm and Tem, Day 0 Axial Inertia and CD4+ Tem, as well as Day 15 Skewness Gabor and Monocytes. Whether these metrics bear clinical significance remains to be determined.

Table 4B
Downregulated at Day 15.

Down at D15	Log2 FC	-log10 P-value
IRF4	-1.0052029	2.525074453
MRGPRF	-1.0120462	2.942244031
MFAP4	-1.0125946	2.054220646
SPARC	-1.0142874	3.150902662
IGFBP6	-1.0158667	2.495205134
ADGRF4	-1.0174452	3.259581059
MTRNR2L6	-1.0191197	1.599039669
SLC51B	-1.0235564	2.268568256
MMP2	-1.0281927	2.773431815
AKR1B10	-1.0344428	1.670883369
MYOCD	-1.0365763	2.028046942
THY1	-1.0391114	2.621289245
SELE	-1.0405125	1.823426733
CD79A	-1.0413398	2.093533301
ANGPTL2	-1.0461687	2.938833255
POSTN	-1.046519	2.262130056
APLNR	-1.0483134	2.471178791
FOLH1	-1.0541064	1.772971205
CIDEC	-1.0554174	1.653504707
WNT5B	-1.0566446	2.55262788
SLC16A9	-1.0966196	1.619174347
IGHM	-1.0967334	1.884794032
SCARA5	-1.108745	1.54688833
ACSL6	-1.111459	1.754581992
RPL17-C18orf32	-1.1125784	2.524504185
DHRS9	-1.1141819	1.872895817
ECHDC3	-1.1161149	2.270188937
APOC4-APOC2	-1.1263141	1.900024169
PLVAP	-1.1332881	3.06794862
GPNMB	-1.1352284	3.664109387
JCHAIN	-1.1370655	1.62364527
EGF	-1.1376875	1.924347717
IGFBP5	-1.1395728	3.21455477
IGLV2–11	-1.148493	1.618335885
CD248	-1.1493039	3.021704256
RSPO3	-1.1535568	1.864184923
ERP27	-1.1614245	2.582900227
CCR3	-1.1694047	3.217752578
IGKV2–30	-1.1941144	1.681192448
ACTA2	-1.1970454	4.49928712
IGHG1	-1.2107732	1.962033523
ACTG2	-1.2152384	2.745414257
IGHV3–48	-1.2303015	1.827765005
IGLV3–21	-1.2342393	1.873199158
CDH16	-1.2434097	1.812603829
IGKV1–17	-1.253521	1.524280242
CEACAM7	-1.2626239	1.932653737
MTRNR2L3	-1.2878544	2.095081748
IGLC3	-1.2906071	1.862799815
IGKV2–24	-1.2956172	2.145444145
VIP	-1.3131165	1.651734347
VSTM2L	-1.323814	2.043664779
IGKV1–6	-1.3240729	2.002900646
HOXA13	-1.3296355	1.656332266
IGHV3–53	-1.3424375	2.130490788
IGKV3D-20	-1.35321	1.677892605
IGKV1–12	-1.3641773	2.081662007
IGKV1–16	-1.3817283	1.941124043
IGLC1	-1.3935728	2.694382558
MTRNR2L10	-1.4003055	1.998647359
KDR	-1.4025695	1.568644145
IGKV6–21	-1.4147421	1.740210217
IGKC	-1.4157543	2.594030013
IGLL5	-1.4187499	2.507796152
IGKV4–1	-1.4409644	2.768508826
IGHV3–73	-1.4418694	1.570014668
IGKV3–20	-1.4545121	2.830582436
MTRNR2L1	-1.4550349	1.578354697
IGLV7–43	-1.4604215	2.373510675
IGHA1	-1.4611654	2.622593081
IGKV2–28	-1.4647695	2.777629778
SLC26A3	-1.4737395	1.649104433
IGHV3–11	-1.4836573	1.874766836
ST6GAL2	-1.4898095	2.121486915
HLA-DMB	-1.4944375	1.717111036
IGKV1–5	-1.5169146	2.559764374
CCL11	-1.5214294	3.484274754
IGHG4	-1.530975	2.040686015
IGLV1–51	-1.5310012	3.087478079
IGLV2–23	-1.5489729	2.871693834
IGLV3–25	-1.5744331	3.15304392
IGHV4–59	-1.5779991	3.031040505
IGHV2–5	-1.5983584	3.007858465
IGHV3–30	-1.5992702	2.666617118
CACNG4	-1.6065297	1.900828692
IGKV1–33	-1.6273115	2.72498484
IGLV4–69	-1.6444541	3.156002586
IGLV2–18	-1.6446853	2.17829353
IGLC2	-1.6737573	3.654131957
IGHV4–4	-1.6957483	2.924648242
IGLV1–47	-1.7014071	3.262967747
ZIC2	-1.7390915	2.053963086
IGHV5–51	-1.7481311	2.615308652
IGLV3–19	-1.7565623	3.295168634
IGKV1D-39	-1.761169	2.587092144
IGLV8–61	-1.7671028	3.047943054
LY75-CD302	-1.7711289	4.457798281
HOXD13	-1.7741166	2.176758891
IGKV3–11	-1.7756773	3.334433436
IGLV7–46	-1.7833271	3.06497251
IGKV1–39	-1.7863222	1.92163447
IGLV3–9	-1.788492	3.312014113
CST1	-1.7886692	2.344909196
MTRNR2L11	-1.8030634	2.40551266
IGLV1–40	-1.8307265	3.906063503
IGHV3–23	-1.844605	3.853615827
IGHV3–49	-1.8546938	3.085379508
IGKV1D-16	-1.8627109	2.163347892
IGKV1D-13	-1.8833867	2.675205771
IGLV3–1	-1.8879636	3.626999793
IGHV3–33	-1.9086467	1.999448262
IGHV1–3	-1.9135656	2.397307295
IGKV1–27	-1.9222628	3.014874821
INSL5	-1.9495226	1.573995171
IGHV1–18	-1.9641615	1.909746698
IGHV4–39	-1.990833	2.046879275
MTRNR2L12	-1.9934478	1.945092544
IGLV6–57	-2.0423464	3.319596114
IGKV3–15	-2.0506431	3.424700534
IGHV1–69D	-2.1146963	1.868207332
CEP20	-2.1985611	2.118067522
IGHV3–21	-2.3034741	1.884054109
MTRNR2L8	-2.3608605	2.584743458
HLA-DQB1	-2.5370577	1.518189019
IGHV3–15	-2.63408	2.181811695
IGHV1–69	-2.6890022	3.409251187
FGF2	-2.7152405	3.370161905
IGLV1–44	-3.0393683	2.558370919

CMS subtypesand treatmentresponse

We next performed consensus molecular subtype (CMS) classification at baseline and day 15. CMS subtype distributions vary based on location in the colon/rectum. For example, MSI-high, hypermutated CMS1 subtype tumors are most frequently found in the right colon (31 % of right colon tumors) and are found least frequently in the rectum, comprising just 3 % of rectal tumors. In our study, baseline CMS classification distribution was consistent with these reports (Fig. 4A). CMS1 phenotype represented 5 % of tumors, CMS2 13.5 %, CMS3 16 %, and CMS4 35 %, while 30 % did not segregate into a CMS classification (Fig. 4A). After 2 weeks of TGFβ inhibition, CMS classifications were altered (Fig. 4B-C). There was a decrease in CMS4 classification (35 % to 19 %, Figs. 4A-B), consistent with a reduction in TGFβ activation. There was an increase in CMS2 and CMS3 classification (Figs. 4A-B). Change in CMS classification by patient suggests that many patients with CMS4 baseline classification altered phenotypes towards a nonclassified (NA)

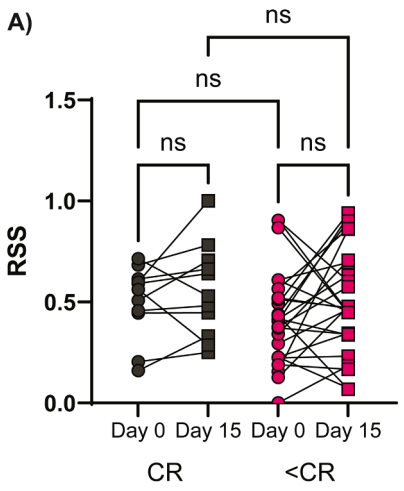

B) i)

Day 0	RSS Prediction	
	<CR	CR
<CR	17 (68%)	8 (32%)
CR	4 (36%)	7 (64%)

FET p=0.1410

ii)

Day 15	RSS Prediction	
	<CR	CR
<CR	15 (60%)	10 (40%)
CR	5 (42%)	7 (58%)

FET p=0.4821

iii)

Combined	RSS Prediction	
	<CR	CR
<CR	32 (78%)	18 (22%)
CR	9 (56%)	14 (44%)

FET p=0.0746

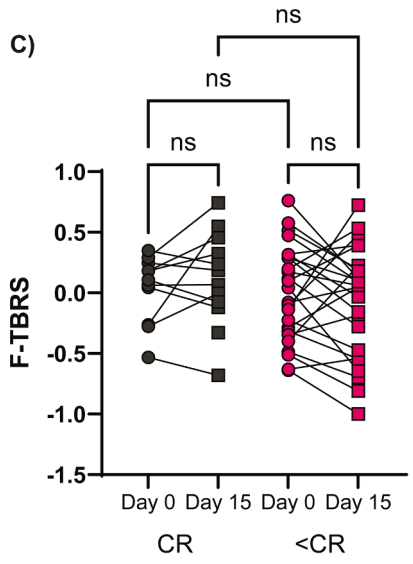

D) i)

Day 0	F-TBRS	
	High/Med	Low
CR	10 (91%)	1 (9%)
<CR	20 (80%)	5 (20%)

FET p=0.6428

ii)

Day 15	F-TBRS	
	High/Med	Low
CR	11 (92%)	1 (8%)
<CR	18 (72%)	7 (28%)

FET p=0.2323

iii)

Combined	F-TBRS	
	High/Med	Low
CR	21 (91%)	2 (9%)
<CR	38 (76%)	12 (24%)

FET p=0.2005

Fig. 2. Radiosensitivity score (RSS) and fibroblast TGFβ response score (F-TBRS) associations with response. A) RSS at baseline (Day 0) and Day 15 in patients with CR vs <CR. B) Response predictions of RSS using cutoff of 0.5 at i) Day 0, ii) Day 15, or iii) Combined across all time points. Fisher exact test (FET) listed for each. C) F-TBRS at Day 0 and Day 15 in patients with CR vs <CR. D) Association between low vs high/medium F-TBRS and CR vs <CR at i) Day 0, ii) Day 15, or iii) Combined across all time points. Fisher exact test (FET) listed for each.

expression pattern or CMS3 pattern (Fig. 4C). The increase in CMS2 phenotype at day 15 was primarily related to unclassified (NA) tumors at day 0 (Fig. 4C).

With the addition of CMS phenotype, we evaluated whether RNA-based cell quantifications or MRI based features were able to cluster patients by CMS phenotype or treatment response (CR vs <CR). Principal component analysis and hierarchical clustering failed to identify patients based on CMS phenotype or treatment response at baseline or after TGFβ inhibition using (**Supplementary Figures 6A-B** (CIBERSORT), **7A-B** (MCPcounter), **8A-B** (xCell)). MRI features also failed to correlate with molecular subtype or response at baseline (**Supplementary Figure 9A**) or after galunisertib (**Supplementary Figure 9B**). Since our original publication failed to show an association between immune cell density and response, the cellular deconvolution data are not entirely surprising. However, we have previously shown a correlation between MRI parameters and chemoradiation response, but those parameters included both the texture features presented here combined with deformation features, which we did not include in this analysis as those features did not correlate with immune cell counts in the prior analysis. Therefore, the limitations in grouping CMS subtype or response by MRI features may be due to the omission of these data.

Finally, we evaluated whether specific CMS phenotypes were associated with response. Complete responders had predominately CMS3 and CMS4 classifications at baseline and after TGFβ inhibition (Fig. 4D). CMS3 and CMS4 phenotype were positively correlated with complete response (p=0.0321, Fig. 4E). This is particularly notable as the CMS4 phenotype is typically poorly responsive to neoadjuvant chemoradiation in rectal cancer*(2,* [31]. When evaluated individually (e.g. CMS4 vs all others) there was no individual CMS category that associated with complete response. There was a trend that favored complete response in males with CMS3 and CMS4 phenotype (p=0.0923, Fig. 4F), whereas <CR patients had equal distribution of males and females across CMS subtypes (Fig. 4G). These data suggest the strongest benefit of galunisertib was observed amongst patients with CMS3 and CMS4 phenotypes, while CMS2 patients did not appear to benefit.

Discussion

Improving response to neoadjuvant therapy for patients with locally advanced rectal cancer has the potential to improve organ preservation, quality of life, and disease-free survival[1,5,32]. Molecular classification of tumors has the potential to stratify patients based on tumor

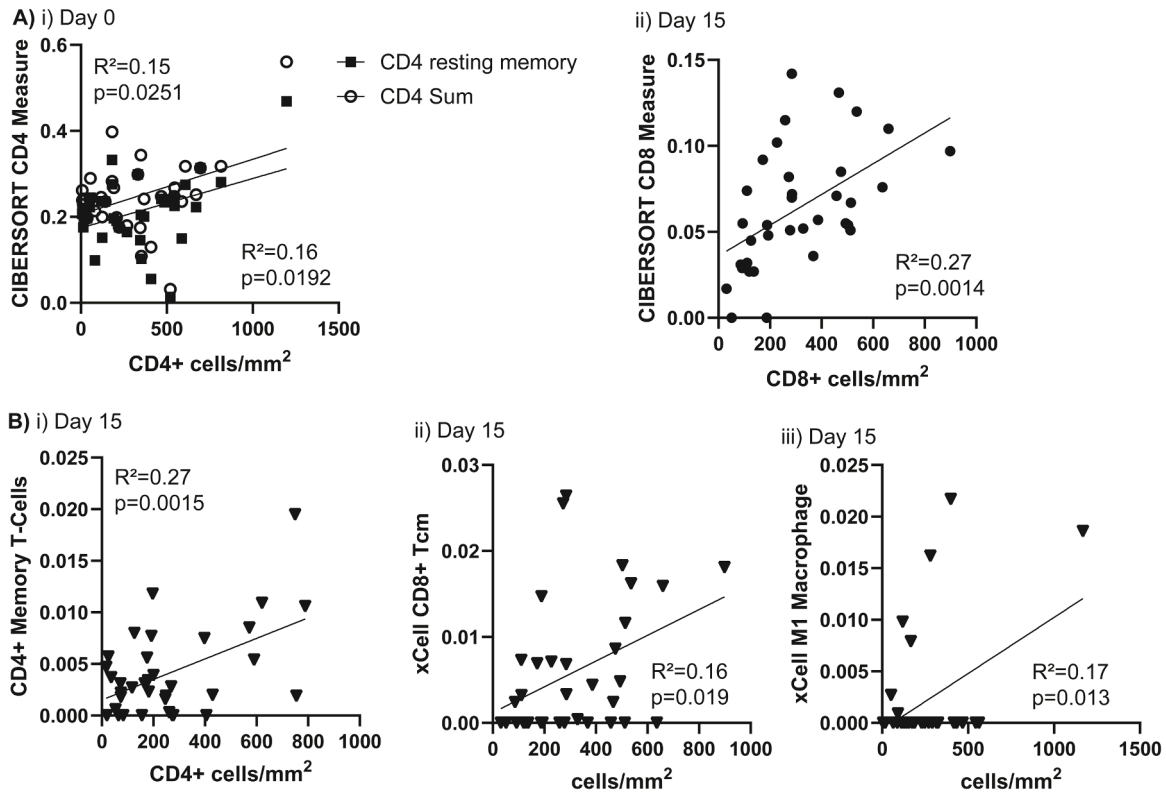

Fig. 3. RNA based cell counts and their correlation with quantitative immunohistology measures. A) CIBERSORT cell classifications associate with immune infiltrate measures by immunohistology for i) CD4+ cells at Day 0 and ii) CD8+ T cells at Day 15. B) xCell measures of i) CD4+ Memory T cells, ii) CD8+ central memory (Tcm), and iii) M1 macrophages at day 15 associate with immunohistology measures.

biology and therapeutic response. The consensus molecular subgroups for colorectal cancer have correlated with response to neoadjuvant chemoradiation, with CMS1 demonstrating higher probability of complete response, while CMS4 demonstrating the lowest probability of complete response*(2,* [7]. Patients with CMS4 phenotypes have the poorest prognosis, with worse disease-free and overall survival. Retrospective analyses suggest patients with CMS4 tumors respond better to irinotecan containing chemotherapy regimens vs oxaliplatin[33], but outcomes are still poor. Preclinical modeling using patient-derived xenografts demonstrated improved response in the chemoresistant CMS4 subtype when 5-FU chemotherapy was combined with HSP90 inhibitor, luminespib, which was not observed in the chemosensitive CMS2 xenografts[34]. Similarly, HSP90 inhibitors have also shown promise as radiation sensitizers in radioresistant cell lines[35], though this has not been tested across tumors from differing CMS subtypes. Our data suggests that targeting one of the key biologic drivers of CMS4 phenotype, TGFβ, with galunisertib resulted in altered gene expression patterns and improved response to chemoradiation.

One of the factors limiting the successful translation of TGFβ inhibitors to the clinic has been challenges with patient selection. These data provide key biologic rationale for patient selection or trial stratification. TGFβ is a critical driver to epithelial-to-mesenchymal transition, which has been associated with poor response to chemoradiation *(2)* and immune checkpoint blockade[36]. Enriching for stromal-rich or EMT gene signatures in trials of TGFβ inhibitors, may be one strategy to select for patients with the highest probability of response. While baseline TGFβ response signatures failed to correlate with response, these may reflect genes acutely altered by the presence of TGFβ, while the stromal-rich phenotype or EMT signatures may reflect prolonged TGFβ exposure, and are therefore more likely to benefit from galunisertib therapy. Medium or high TGFβ response signatures, when combined across timepoints, did correlate with response to treatment. This may also suggest prolonged TGFβ signaling or simply reflect higher power to detect differences when more data points are included in the analysis. Both the stromal TGFβ response signatures (E-TBRS and M-TBRS) and CMS4 phenotype, could be implemented for better patient selection for TGFβ inhibitors, a key barrier faced clinically.

We also saw complete response in patients with baseline CMS3 and non-distinct (NA) phenotypes, but not in CMS1 and CMS2 where response to chemoradiation alone would be predicted to be greater. Based on these data, if we move forward with the addition of a TGFβ inhibitor in neoadjuvant rectal cancer treatment, we would favor excluding CMS1 and CMS2 patients, the former of which would now likely receive immune checkpoint blockade[37], and the latter which may not benefit from the addition of TGFβ blockade. Since RNAseq-based stratification methods are cost and time prohibitive in many community settings, adoption of histology-based classifications, such as the imCMS, may provide a readily adaptable approach to identifying and stratifying patient treatments[31]. Importantly, we found that CMS phenotypes are dynamic, with reclassification occurring for most patients. We do not have an untreated cohort to compare to, so it remains unknown whether CMS classifications change in the absence of treatment, based on differences in sampling or tumor evolution. Therefore, further evaluation of CMS as a stratification strategy is warranted. Additionally, while we demonstrated alterations in gene signatures, monotherapy with TGFβ inhibitors alone may not be sufficient to reduce tumor burden. Similar to using HSP90 inhibition as a chemosensitizer[34], TGFβ inhibition may be viewed as a sensitizer to chemotherapy, radiation, and/or immunotherapy. Ongoing trials combining TGFβ targeting strategies with immune checkpoint blockade (NCT06788990 and NCT06603844), or chemoradiation (NCT06044311 and NCT06767813) may provide further data to support patient selection criteria.

MYC is a proto-oncogene required for normal intestinal epithelial renewal. However, *MYC* overexpression is present in up to 80 % of colorectal cancers. APC mutations increase β-catenin mediated

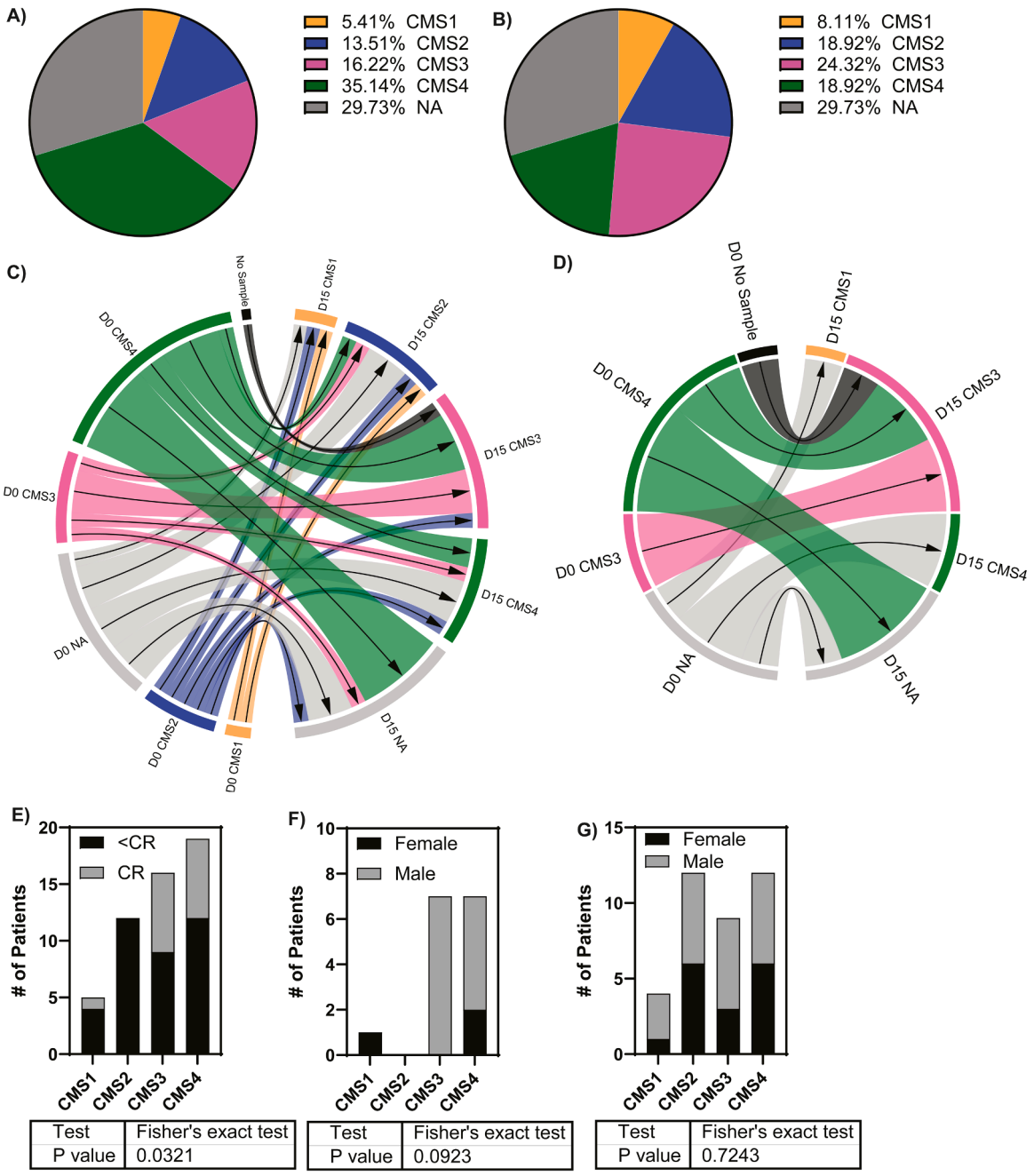

Test	Fisher's exact test
P value	0.0321

Test	Fisher's exact test
P value	0.0923

Test	Fisher's exact test
P value	0.7243

Fig. 4. CMS phenotypes 3 and 4 correlate with response to neoadjuvant chemoradiation with Galunisertib. A) CMS phenotypes at baseline (Day 0). B) CMS phenotypes after 2 weeks of galunisertib at Day 15. Migration of CMS phenotypes between Day 0 and Day 15 in all patients (C) and exclusively within CR (D). E) Relationship between CR and CMS phenotype. Fisher's exact test value below. F) Association of sex with CMS phenotype in CR. G) Association of sex with CMS phenotype in <CR.

transcription of *MYC*. *MYC* regulates global metabolic reprogramming of colorectal cancers, and inhibition of pyrimidine synthesis genes can overcome *MYC* overexpression[38]. MYC also plays a role in ER stress promoting the unfolded protein response pathway[39]. Prolonged ER stress can lead to immunogenic cell death. *MYC* expression has positively correlated with response to chemoradiation*(2,* [40]. Interestingly, baseline samples from patients with complete response had low *MYC* expression, but after 2 weeks of galunisertib, they exhibited *MYC* overexpression. These data suggest low *MYC* expression may be an indirect selection criteria for patients who might respond better to galunisertib + chemoradiation.

Our study was exploratory in nature, and with a small sample size, and we should exercise caution in interpreting the data. While we were able to see changes in CMS classification, differential gene expression, and transcription factor activity with just 2 weeks of galunisertib, given heterogeneity of patient samples and the number of comparisons employed, few significant differences remained after correction for multiple testing. Multimodal measurements including imaging and cellular component analyses remain largely descriptive and provide a basis for further investigation. Despite high levels of variability, consistent patterns were observed with similar biologic pathways altered, which support our hypothesis that TGFβ drives a stromal radioresistant phenotype which can be overcome by addition of galunisertib to chemoradiation.

Data Sharing Statement: Since this involves patient data, any unaligned or aligned sequencing reads are considered PHI and will not be

shared. De-identified RNA counts are available at GEO Accession Viewer **(**GSE318268**).**

SUPP

Supplementary Figure 1. Trial Schema. Enrolled patients completed a 14-day course of Galunisertib, followed by chemoradiation with continuous infusion 5-fluorouracil or capecitabine with radiation to 50.4–54 Gy in 28–30 fractions. On day 30, patients underwent another 14-day course of Galunisertib concurrent with chemoradiation. Five to nine weeks after completing their neoadjuvant therapy, patients underwent a response assessment. Those with complete response by physical exam, proctoscopy, and MRI, could opt for non-operative management and proceed to mFOLFOX6. Those with less than a complete response underwent surgical resection. The primary endpoint was complete response rate, which was a composite of pathologic complete responses from those patients who proceeded to surgery, and clinical complete responses maintained at 1 year after completion of therapy for those who chose non-operative management. Forceps biopsy and MRI were obtained at baseline (day 0) and after first course of galunisertib (day 15). Created using BioRender.

Supplementary Figure 2. Differentially expressed genes and pathways associated with complete responders. Volcano plots of differentially expressed genes between CR and <CR at A) baseline (D0) with B) hallmark pathway analysis for differentially expressed genes. Volcano plots of differentially expressed genes between CR and <CR at C) day 15 (D15) with D) hallmark pathway analysis for differentially expressed genes. E) Difference in gene expression between day 15 and day 0 in all patients regardless of response. F) Hallmark pathway analysis corresponding to E. For volcano plots, upregulated genes in CR (A, C) or at day 15 (E) shown on right (blue), downregulated genes shown on the left (red). Individual genes highlighted in Tables 1–4. For pathway analysis, upregulated pathways are shown in red, size of circle reflects size of effect.

Supplementary Figure 3. Myc transcription factor activity at baseline and day 15 associate complete response. A) Transcription factor activity score differences between complete responders (CR) and less than complete responders (Non-CR) at baseline (D0). B) Differentially expressed genes between CR and non-CR at D0. Genes positively associated with Myc transcription factor are red, while genes negatively associated with Myc activity are blue. C) Transcription factor activity score differences between CR and Non-CR at after galunisertib (D15). D) Differentially expressed genes between CR and non-CR at D15

Supplementary Figure 4. TGFβ response signatures do not associate with treatment response. A) T cell TGFβ response signature (T-TBRS) does not correlate with treatment complete response (CR) or <CR. B) Proportion of patients with high/medium score vs low score at i) baseline, ii) day 15, or iii) all time points combined. Fisher exact test (FET) values as indicated. C) Macrophage TGFβ response signature (M-TBRS) for CR and <CR at indicated time points. D) Proportion of patients with high/medium score vs low score at i) baseline, ii) day 15, or iii) all time points combined. FET values as indicated. E) Endothelial TGFβ response signature (E-TBRS) for CR and <CR at indicated time points. D) Proportion of patients with high/medium score vs low score at i) baseline, ii) day 15, or iii) all time points combined. FET values as indicated. ns=not significant

Supplementary Figure 5. Correlation between RNA based cell quantification and MRI-based measures of the tumor microenvironment. Uncorrected Pearson Correlation coefficients for association between indicated cell types and MRI features using A) CIBERSORT, B) MCPcounter, or C) xCell based cell quantification methods. *$p<0.05$, **$p<0.01$, ***$p<0.001$, ****$p<0.0001$. White squares indicate insufficient data to correlate.

Supplementary Figure 6. CIBERSORT cell quantification. A) Baseline (Day 0) i) principal component analysis and ii) hierarchical clustering failed to discriminate patients based on CMS classifier or treatment response (CR vs <CR). B) After 2 weeks of galunisertib (Day 15) i) PCA and ii) hierarchical clustering were still unable to discriminate patients based on CMS classifier or treatment response (CR vs <CR).

Supplementary Figure 7. MCPcounter cell quantification. A) Baseline (Day 0) i) principal component analysis clusters CMS3 and CMS4 together and ii) hierarchical clustering failed to discriminate patients based on CMS classifier or treatment response (CR vs <CR). B) After 2 weeks of galunisertib (Day 15) i) PCA mildly clusters CMS3 and 4 together while ii) hierarchical clustering was still unable to discriminate patients based on CMS classifier or treatment response (CR vs <CR)

Supplementary Figure 8. xCell cell quantification. A) Baseline (Day 0) i) principal component analysis and ii) hierarchical clustering group many CMS3 and 4 patients together but failed to discriminate patients based on CMS classifier or treatment response (CR vs <CR). B) After 2 weeks of galunisertib (Day 15) i) PCA and ii) hierarchical clustering group CMS3 and 4 together, but were still unable to discriminate patients based on CMS classifier or treatment response (CR vs <CR).

Supplementary Figure 9. MRI parameters. A) Baseline (Day 0) i) principal component analysis and ii) hierarchical clustering based on MRI parameters failed to discriminate patients based on CMS classifier or treatment response (CR vs <CR). B) After 2 weeks of galunisertib (Day 15) i) PCA and ii) hierarchical clustering unable to discriminate patients based on CMS classifier or treatment response (CR vs <CR).

CRediT authorship contribution statement

Venkatesh Rajamanickam: Writing – review & editing, Visualization, Validation, Supervision, Software, Resources, Project administration, Methodology, Formal analysis, Data curation. **Noah D. Simons:** Writing – review & editing, Visualization, Validation, Software, Investigation, Formal analysis. **Wesley Rosales:** Writing – review & editing, Visualization, Validation, Software, Investigation, Formal analysis. **Anton Kravchenko:** Writing – review & editing, Visualization, Validation, Software, Investigation, Formal analysis. **Tomoko Yamazaki:** Writing – review & editing, Validation, Supervision, Software, Resources, Project administration, Methodology, Investigation, Formal analysis, Data curation, Conceptualization. **Brady Bernard:** Writing – review & editing, Visualization, Validation, Supervision, Software, Resources, Project administration, Methodology, Formal analysis, Data curation. **Brian Piening:** Writing – review & editing, Visualization, Validation, Supervision, Software, Resources, Project administration, Methodology, Formal analysis, Data curation. **Enric Domingo:** Writing – review & editing, Software, Data curation. **Timothy Maughan:** Writing – review & editing, Supervision, Project administration, Formal analysis, Data curation. **Charlems Alvarez-Jimenez:** Writing – review & editing, Visualization, Validation, Software, Investigation, Formal analysis. **Thomas Desilvio:** Writing – review & editing, Visualization, Validation, Software, Investigation, Formal analysis. **Satish Viswanath:** Writing – review & editing, Visualization, Validation, Supervision, Software, Project administration, Investigation, Formal analysis. **Mark Whiteford:** Writing – review & editing, Investigation, Data curation. **Amanda Hayman:** Writing – review & editing, Investigation, Data curation. **David O'Brien:** Writing – review & editing, Investigation, Data curation. **Maria X. Kiely:** Writing – review & editing, Investigation, Data curation. **Rehan Ahmad:** Writing – review & editing, Investigation, Data curation. **Michael J. Gough:** Writing – review & editing, Visualization, Conceptualization. **Marka R. Crittenden:** Writing – review & editing, Visualization, Conceptualization. **Kristina H. Young:** Writing – review & editing, Writing – original draft, Visualization, Validation, Supervision, Resources, Project administration, Methodology, Investigation, Funding acquisition, Formal analysis, Data curation, Conceptualization.

Declaration of competing interest

KHY received funding from Eli Lilly and Company through the ExIST mechanism that partially funded the clinical trial reported herein. KHY was a scientific advisor for Synthis Therapeutics for their TGFβ pipeline. KHY has a sponsored research agreement with Bicara. KHY served as a consultant for Corbus Pharmaceuticals and had an MTA to test their compound preclinically.

Acknowledgements

Primary clinical trial partially funded by Eli Lilly and Company through the ExIST platform. Additional funding support from the Providence Foundation.

Supplementary materials

Supplementary material associated with this article can be found, in the online version, at doi:10.1016/j.tranon.2026.102690.

References

[1] S.T. Martin, H.M. Heneghan, D.C. Winter, Systematic review and meta-analysis of outcomes following pathological complete response to neoadjuvant chemoradiotherapy for rectal cancer, Br. J. Surg. 99 (2012) 918–928.
[2] R. Sauer, H. Becker, W. Hohenberger, C. Rödel, C. Wittekind, R. Fietkau, P. Martus, J. Tschmelitsch, E. Hager, C.F. Hess, J.-H.H. Karstens, T. Liersch, H. Schmidberger, R. Raab, Preoperative versus postoperative chemoradiotherapy for rectal cancer, N. Engl. J. Med. 351 (2004) 1731–1740.
[3] J. Garcia-Aguilar, D.D. Smith, K. Avila, E.K. Bergsland, P. Chu, R.M. Krieg, Timing of rectal cancer response to Chemoradiation Consortium, optimal timing of surgery after chemoradiation for advanced rectal cancer: preliminary results of a multicenter, nonrandomized phase II prospective trial, Ann. Surg. 254 (2011) 97–102.
[4] E. Fokas, M. Allgäuer, B. Polat, G. Klautke, G.G. Grabenbauer, R. Fietkau, T. Kuhnt, L. Staib, T. Brunner, A.-L. Grosu, W. Schmiegel, L. Jacobasch, J. Weitz, G. Folprecht, A. Schlenska-Lange, M. Flentje, C.-T. Germer, R. Grützmann, M. Schwarzbach, V. Paolucci, W.O. Bechstein, T. Friede, M. Ghadimi, R.-D. Hofheinz, C. Rödel, German rectal cancer Study group, randomized phase II trial of chemoradiotherapy plus induction or consolidation chemotherapy as total neoadjuvant therapy for locally advanced rectal cancer: CAO/ARO/AIO-12, J. Clin. Oncol. 37 (2019) 3212–3222.
[5] F.S. Verheij, D.M. Omer, H. Williams, S.T. Lin, L.-X. Qin, J.T. Buckley, H. M. Thompson, J.B. Yuval, J.K. Kim, R.F. Dunne, J. Marcet, P. Cataldo, B. Polite, D. O. Herzig, D. Liska, S. Oommen, C.M. Friel, C. Ternent, A.L. Coveler, S. Hunt, A. Gregory, M.G. Varma, B.L. Bello, J.C. Carmichael, J. Krauss, A. Gleisner, J. G. Guillem, L. Temple, K.A. Goodman, N.H. Segal, A. Cercek, R. Yaeger, G.M. Nash, M. Widmar, I.H. Wei, E.P. Pappou, M.R. Weiser, P.B. Paty, J.J. Smith, A.J. Wu, M. J. Gollub, L.B. Saltz, J. Garcia-Aguilar, Long-term results of organ preservation in patients with rectal adenocarcinoma treated with total neoadjuvant therapy: the randomized phase II OPRA trial, J. Clin. Oncol. 42 (2024) 500–506.
[6] J. Guinney, R. Dienstmann, X. Wang, A. de Reyniès, A. Schlicker, C. Soneson, L. Marisa, P. Roepman, G. Nyamundanda, P. Angelino, B.M. Bot, J.S. Morris, I. M. Simon, S. Gerster, E. Fessler, F. De Sousa E Melo, E. Missiaglia, H. Ramay, D. Barras, K. Homicsko, D. Maru, G.C. Manyam, B. Broom, V. Boige, B. Perez-Villamil, T. Laderas, R. Salazar, J.W. Gray, D. Hanahan, J. Tabernero, R. Bernards, S.H. Friend, P. Laurent-Puig, J.P. Medema, A. Sadanandam, L. Wessels, M. Delorenzi, S. Kopetz, L. Vermeulen, S. Tejpar, The consensus molecular subtypes of colorectal cancer, Nat. Med. 21 (2015) 1350–1356.
[7] U. Mahmood, A. Blake, S. Rathee, L. Samuel, G. Murray, D. Sebag-Montefiore, S. Gollins, N.P. West, R. Begum, S.P. Bach, S.D. Richman, P. Quirke, K.L. Redmond, M. Salto-Tellez, V.H. Koelzer, S.J. Leedham, I. Tomlinson, P.D. Dunne, F.M. Buffa, S:CORT consortium, T.S. Maughan, E. Domingo, Stratification to neoadjuvant radiotherapy in rectal cancer by regimen and transcriptional signatures, Cancer Res. Commun 4 (2024) 1765–1776.
[8] J. Galon, A. Costes, F. Sanchez-Cabo, A. Kirilovsky, B. Mlecnik, C. Lagorce-Pagès, M. Tosolini, M. Camus, A. Berger, P. Wind, F. Zinzindohoué, P. Bruneval, P.-H. Cugnenc, Z. Trajanoski, W.-H. Fridman, F. Pagès, Type, density, and location of immune cells within human colorectal tumors predict clinical outcome, Science 313 (2006) 1960–1964.
[9] M. Anitei, G. Zeitoun, B. Mlecnik, F. Marliot, N. Haicheur, A. Todosi, A. Kirilovsky, C. Lagorce, G. Bindea, D. Ferariu, M. Danciu, P. Bruneval, V. Scripcariu, J.-M. Chevallier, F. Zinzindohoué, A. Berger, J. Galon, F. Pagès, Prognostic and predictive values of the immunoscore in patients with rectal cancer, Clin. Cancer Res. 20 (2014) 1891–1899.
[10] I.J. Park, S. An, S.Y. Kim, H.M. Lim, S.M. Hong, M.J. Kim, Y.J. Kim, C.S. Yu, Prediction of radio-responsiveness with immune-profiling in patients with rectal cancer, Oncotarget 8 (2017) 79793–79802.
[11] E. Domingo, S. Rathee, A. Blake, L. Samuel, G. Murray, D. Sebag-Montefiore, S. Gollins, N. West, R. Begum, S. Richman, P. Quirke, K. Redmond, A. Chatzipli, A. Barberis, S. Hassanieh, U. Mahmood, M. Youdell, U. McDermott, V. Koelzer, S. Leedham, I. Tomlinson, P. Dunne, S:CORT consortium, F.M. Buffa, T. S. Maughan, A. Blake, F.M. Buffa, E. Domingo, G. Higgins, C. Holmes, V. Koelzer, S. Leedham, T.S. Maughan, G. McKenna, J. Robineau, I. Tomlinson, M. Youdell, P. Quirke, S. Richman, D. Sebag-Montefiore, M. Seymour, N. West, P. Dunne, R. Kennedy, M. Lawler, K. Redmond, M. Salto-Tellez, P. Campbell, A. Chatzipli, C. Hardy, U. McDermott, S. Bach, A. Beggs, J.-B. Cazier, G. Middleton, D. Morton, C. Whalley, L. Brown, R. Kaplan, G. Murray, R. Wilson, R. Adams, R. Sullivan, L. Samuel, P. Harkin, S. Walker, J. Hill, C.-H. Wu, D. Horgan, F.M. Buffa, T. S. Maughan, Identification and validation of a machine learning model of complete response to radiation in rectal cancer reveals immune infiltrate and tgfβ as key predictors, eBioMedicine 106 (2024) 105228.
[12] R.J. Akhurst, A. Hata, Targeting the tgfβ signalling pathway in disease, Nat. Rev. Drug Discov. 11 (2012) 790–811.
[13] D.A. Thomas, J. Massagué, TGF-beta directly targets cytotoxic T cell functions during tumor evasion of immune surveillance, Cancer Cell 8 (2005) 369–380.
[14] A.J. Gunderson, T. Yamazaki, K. McCarty, N. Fox, M. Phillips, A. Alice, T. Blair, M. Whiteford, D. O'Brien, R. Ahmad, M.X. Kiely, A. Hayman, T. Crocenzi, M. J. Gough, M.R. Crittenden, K.H. Young, TGFβ suppresses CD8+ T cell expression of CXCR3 and tumor trafficking, Nat. Commun. 11 (2020) 1749.
[15] L. Gorelik, R.A. Flavell, N. Haven, Abrogation of TGFbeta signaling in T cells leads to spontaneous T cell differentiation and autoimmune disease, Immunity 12 (2000) 171–181.
[16] R. a Flavell, S. Sanjabi, S.H. Wrzesinski, P. Licona-Limón, The polarization of immune cells in the tumour environment by TGFbeta, Nat. Rev. Immunol. 10 (2010) 554–567.
[17] S. Mariathasan, S.J. Turley, D. Nickles, A. Castiglioni, K. Yuen, Y. Wang, E.E.K. Iii, H. Koeppen, J.L. Astarita, R. Cubas, S. Jhunjhunwala, R. Banchereau, Y. Yang, Y. Guan, C. Chalouni, J. Ziai, Y. Şenbabaoğlu, S. Santoro, D. Sheinson, J. Hung, J. M. Giltnane, A.A.K. Pierce, K. Mesh, S. Lianoglou, J. Riegler, R.A.D.D. Carano, P. Eriksson, M. Hoglund, L. Somarriba, D.L. Halligan, M. Van Der Heijden, Y. Loriot, J.E. Rosenberg, L. Fong, I. Mellman, D.S. Chen, M. Green, C. Derleth, G. D. Fine, P.S. Hegde, R. Bourgon, T. Powles, E.E. Kadel, H. Koeppen, J.L. Astarita, R. Cubas, S. Jhunjhunwala, R. Banchereau, Y. Yang, Y. Guan, C. Chalouni, J. Ziai, Y. Şenbabaoğlu, S. Santoro, D. Sheinson, J. Hung, J.M. Giltnane, A.A.K. Pierce, K. Mesh, S. Lianoglou, J. Riegler, R.A.D.D. Carano, P. Eriksson, M. Höglund, L. Somarriba, D.L. Halligan, M.S. Van Der Heijden, Y. Loriot, J.E. Rosenberg, L. Fong, I. Mellman, D.S. Chen, M. Green, C. Derleth, G.D. Fine, P.S. Hegde, R. Bourgon, T. Powles, TGFβ attenuates tumour response to PD-L1 blockade by contributing to exclusion of T cells, Nature 554 (2018) 544–548.
[18] K.H. Young, P. Newell, B. Cottam, D. Friedman, T. Savage, J.R. Baird, E. Akporiaye, M.J. Gough, M. Crittenden, TGFβ inhibition prior to hypofractionated radiation enhances efficacy in preclinical models, Cancer Immunol. Res. (2014), https://doi.org/10.1158/2326-6066.CIR-13-0207.
[19] T. Yamazaki, A.J. Gunderson, M. Gilchrist, M. Whiteford, M.X. Kiely, A. Hayman, D. O'Brien, R. Ahmad, J.V Manchio, N. Fox, K. McCarty, M. Phillips, E. Brosnan, G. Vaccaro, R. Li, M. Simon, E. Bernstein, M. McCormick, L. Yamasaki, Y. Wu, A. Drokin, T. Carnahan, Y. To, W.L. Redmond, B. Lee, J. Louie, E. Hansen, M. C. Solhjem, J. Cramer, W.J. Urba, M.J. Gough, M.R. Crittenden, K.H. Young, Galunisertib plus neoadjuvant chemoradiotherapy in patients with locally advanced rectal cancer: a single-arm, phase 2 trial, Lancet Oncol (2022), https://doi.org/10.1016/S1470-2045(22)00446-6.
[20] C. Alvarez-Jimenez, J.T. Antunes, T. DeSilvio, Z. Wei, M. Ismail, J.E. Willis, E. Steinhagen, A. Purysko, D. Liska, S. Krishnamurthi, M. Crittenden, M. Gough, K. Young, A. Madabhushi, E. Romero, P. Tiwari, S.E. Viswanath, A novel structural modeling magnitude and orientation radiomic descriptor for evaluating response to neoadjuvant therapy in rectal cancers via MRI, npj Precis. Oncol. 9 (2025) 215.
[21] R. Patro, G. Duggal, M.I. Love, R.A. Irizarry, C. Kingsford, Salmon provides fast and bias-aware quantification of transcript expression, Nat. Methods 14 (2017) 417–419.
[22] D. Aran, Z. Hu, A.J. Butte, xCell: digitally portraying the tissue cellular heterogeneity landscape, Genome Biol 18 (2017) 220.
[23] A.M. Newman, C.L. Liu, M.R. Green, A.J. Gentles, W. Feng, Y. Xu, C.D. Hoang, M. Diehn, A.A. Alizadeh, Robust enumeration of cell subsets from tissue expression profiles, Nat. Methods 12 (2015) 453–457.
[24] P.K. Kimes, Y. Liu, D.Neil Hayes, J.S. Marron, Statistical significance for hierarchical clustering, Biometrics 73 (2017) 811–821.
[25] M.E. Ritchie, B. Phipson, D. Wu, Y. Hu, C.W. Law, W. Shi, G.K. Smyth, limma powers differential expression analyses for RNA-sequencing and microarray studies, Nucleic Acids Res 43 (2015) e47–e47.
[26] M.D. Robinson, D.J. McCarthy, G.K. Smyth, edgeR: a bioconductor package for differential expression analysis of digital gene expression data, Bioinformatics 26 (2010) 139–140.
[27] P. Badia-i-Mompel, J. Vélez Santiago, J. Braunger, C. Geiss, D. Dimitrov, S. Müller-Dott, P. Taus, A. Dugourd, C.H. Holland, R.O. Ramirez Flores, J. Saez-Rodriguez, M.L. Kuijjer, decoupleR: ensemble of computational methods to infer biological activities from omics data, Bioinforma. Adv. 2 (2022), https://doi.org/10.1093/bioadv/vbac016.
[28] S. Müller-Dott, E. Tsirvouli, M. Vazquez, R.O. Ramirez Flores, P. Badia-i-Mompel, R. Fallegger, D. Türei, A. Lægreid, J. Saez-Rodriguez, Expanding the coverage of regulons from high-confidence prior knowledge for accurate estimation of transcription factor activities, Nucleic Acids Res 51 (2023) 10934–10949.

[29] P.W. Eide, J. Bruun, R.A. Lothe, A. Sveen, CMScaller: an R package for consensus molecular subtyping of colorectal cancer pre-clinical models, Sci. Rep. 7 (2017) 16618.
[30] A. Calon, E. Espinet, S. Palomo-Ponce, D.V.F. Tauriello, M. Iglesias, M.V. Céspedes, M. Sevillano, C. Nadal, P. Jung, X.H.F. Zhang, D. Byrom, A. Riera, D. Rossell, R. Mangues, J. Massagué, E. Sancho, E. Batlle, Dependency of colorectal cancer on a TGF-β-driven program in stromal cells for metastasis initiation, Cancer Cell 22 (2012) 571–584.
[31] M.W. Lafarge, E. Domingo, K. Sirinukunwattana, R. Wood, L. Samuel, G. Murray, S. D. Richman, A. Blake, D. Sebag-Montefiore, S. Gollins, E. Klieser, D. Neureiter, F. Huemer, R. Greil, P. Dunne, P. Quirke, L. Weiss, J. Rittscher, T. Maughan, V. H. Koelzer, Image-based consensus molecular subtyping in rectal cancer biopsies and response to neoadjuvant chemoradiotherapy, npj Precis. Oncol. 8 (2024) 89.
[32] P.A. Custers, M.E. van der Sande, B.A. Grotenhuis, F.P. Peters, S.M.J. van Kuijk, G. L. Beets, S.O. Breukink, A.J.N.M. Bastiaansen, R.G.H. Beets-Tan, M.P. M. Borremans, A.J.A. Bremers, M.S. Dunker, S. Festen, C. Hoff, H.E. Haak, I. L. Huibregtse, M.P.W. Intven, N. Komen, S.A. Koopal, D.M.J. Lambregts, M.E. van Leerdam, M. Maas, C.A.M. Marijnen, J. Melenhorst, K.C.M.J. Peeters, A. Pronk, A. H.W. Schiphorst, I.J.H. Schoenaker, W.H. Schreurs, D.J.A. Sonneveld, A.K. Talsma, B. van Triest, J.B. Tuynman, M. Vermaas, W.H. de Vos tot Nederveen Cappel, D. K. Wasowicz, H.L. van Westreenen, J.H.W. de Wilt, D.D.E. Zimmerman, Long-term quality of life and functional outcome of patients with rectal cancer following a watch-and-wait approach, JAMA Surg. 158 (2023) e230146.
[33] S. ten Hoorn, T.R. de Back, D.W. Sommeijer, L. Vermeulen, Clinical value of consensus molecular subtypes in colorectal cancer: A systematic review and meta-analysis, JNCI J. Natl. Cancer Inst. 114 (2022) 503–516.
[34] A. Sveen, J. Bruun, P.W. Eide, I.A. Eilertsen, L. Ramirez, A. Murumägi, M. Arjama, S.A. Danielsen, K. Kryeziu, E. Elez, J. Tabernero, J. Guinney, H.G. Palmer, A. Nesbakken, O. Kallioniemi, R. Dienstmann, R.A. Lothe, Colorectal cancer consensus molecular subtypes translated to preclinical models uncover potentially targetable cancer cell dependencies, Clin. Cancer Res. 24 (2018) 794–806.
[35] W.-Y. Kim, S.H. Oh, J.-K. Woo, W.K. Hong, H.-Y. Lee, Targeting heat shock protein 90 overrides the resistance of lung cancer cells by blocking radiation-induced stabilization of hypoxia-inducible factor-1alpha, Cancer Res 69 (2009) 1624–1632.
[36] L. Wang, A. Saci, P.M. Szabo, S.D. Chasalow, M. Castillo-Martin, J. Domingo-Domenech, A. Siefker-Radtke, P. Sharma, J.P. Sfakianos, Y. Gong, A. Dominguez-Andres, W.K. Oh, D. Mulholland, A. Azrilevich, L. Hu, C. Cordon-Cardo, H. Salmon, N. Bhardwaj, J. Zhu, M.D. Galsky, EMT- and stroma-related gene expression and resistance to PD-1 blockade in urothelial cancer, Nat. Commun. 9 (2018) 3503.
[37] A. Cercek, M. Lumish, J. Sinopoli, J. Weiss, J. Shia, M. Lamendola-Essel, I.H. El Dika, N. Segal, M. Shcherba, R. Sugarman, Z. Stadler, R. Yaeger, J.J. Smith, B. Rousseau, G. Argiles, M. Patel, A. Desai, L.B. Saltz, M. Widmar, K. Iyer, J. Zhang, N. Gianino, C. Crane, P.B. Romesser, E.P. Pappou, P. Paty, J. Garcia-Aguilar, M. Gonen, M. Gollub, M.R. Weiser, K.A. Schalper, L.A. Diaz, PD-1 blockade in mismatch repair–Deficient, locally advanced rectal cancer, N. Engl. J. Med. 386 (2022) 2363–2376.
[38] K. Satoh, S. Yachida, M. Sugimoto, M. Oshima, T. Nakagawa, S. Akamoto, S. Tabata, K. Saitoh, K. Kato, S. Sato, K. Igarashi, Y. Aizawa, R. Kajino-Sakamoto, Y. Kojima, T. Fujishita, A. Enomoto, A. Hirayama, T. Ishikawa, M.M. Taketo, Y. Kushida, R. Haba, K. Okano, M. Tomita, Y. Suzuki, S. Fukuda, M. Aoki, T. Soga, Global metabolic reprogramming of colorectal cancer occurs at adenoma stage and is induced by MYC, Proc. Natl. Acad. Sci. 114 (2017), https://doi.org/10.1073/pnas.1710366114.
[39] H. Saeed, B.J. Leibowitz, L. Zhang, J. Yu, Targeting Myc-driven stress addiction in colorectal cancer, Drug Resist. Updat. 69 (2023) 100963.
[40] P. Palma, C. Cano, R. Conde-Muiño, A. Comino, P. Bueno, J.A. Ferrón, M. Cuadros, S. Wölfl, Ed. Expression profiling of rectal tumors defines response to neoadjuvant treatment related genes, PLoS One 9 (2014) e112189.